The collapse of the p-f mixing in CeSb with Ni incorporation

1999 J. Phys.: Condens. Matter 11 3687

(http://iopscience.iop.org/0953-8984/11/18/305)

J. Phys.: Condens. Matter **11** (1999) 3687–3697. Printed in the UK PII: S0953-8984(99)97852-9

The collapse of the p–f mixing in CeSb with Ni incorporation

D T Adroja†§, M H Jung†, Y Shibata‡ and T Takabatake‡

† Department of Quantum Matter, ADSM, Hiroshima University, Higashi-Hiroshima 739-8526, Japan

‡ Department of Earth and Planetary Systems Science, Faculty of Science, Hiroshima University, Higashi-Hiroshima 739-8526, Japan

Received 28 September 1998

Abstract. We have synthesized $CeSbNi_{0.15}$ single crystal and measured its magnetic and transport properties. X-ray powder diffraction studies reveal that $CeSbNi_{0.15}$ crystallizes in the cubic structure, like the host CeSb, with Ni atoms occupying interstitial sites. The magnetic susceptibility reveals an antiferromagnetic ordering at $T_N = 9.5$ K. The magnetization isotherm at 1.5 K shows a metamagnetic transition at 6.4 T. The field dependence of the magnetization at 5 K exhibits almost the same behaviour up to a field of 5.5 T for $\boldsymbol{B} \parallel [100]$, $\boldsymbol{B} \parallel [110]$ and $\boldsymbol{B} \parallel [111]$. The resistivity exhibits a sharp rise below T_N which we attribute to the formation of a superzone gap. The obvious effect of Ni incorporation in CeSb is the absence of complex and strong anisotropic magnetic properties. This indicates that the p–f mixing in CeSb is strongly reduced by the incorporation of Ni in the interstitial site. We have also determined the solubility limit of Ni in polycrystalline compounds $CeSbNi_x$ to be $x \approx 0.4$, and studied their magnetic and transport properties. These studies show that T_N for $CeSbNi_x$ alloys varies non-linearly with the Ni content, x.

1. Introduction

Cerium monopnictides CeX (X = P, As, Sb and Bi), having the simple cubic NaCl-type structure, exhibit semimetallic transport properties with very low carrier density (0.01–0.001) per cerium ion [1–4]. The carriers of this system consist of electrons and holes in equal numbers. The transport properties of these compounds are similar to those of typical dense Kondo lattice systems. However, according to a simple Kondo model, the Kondo temperature, T_K, decreases rapidly with decreasing carrier density; hence there should be no observable Kondo effect at any temperature for such low-carrier-density systems [3]. Among these compounds, CeSb and CeBi are well known for their complex magnetic phase diagrams as functions of temperature, magnetic field and pressure, even though their crystal structure is simple [5–7]. For both compounds the paramagnetic-to-antiferromagnetic transition coincides with a cubic-to-tetragonal structural distortion [8]. It is noteworthy that the zero-field heat capacity of CeSb exhibits seven magnetic transitions in a narrow temperature range between 16 K and 8 K, while sixteen magnetic phases have been observed in the B–T phase diagram [2, 5]. The other unusual properties of CeSb are: the coexistence of magnetic and non-magnetic Ce^{3+} planes; the low value of the crystalline-electric-field splitting ($\Delta = 24$–35 K); and the magnetic interactions and strong magnetic anisotropy having the same order [9]. These properties of CeSb have been explained on the basis of the non-linear p–f mixing model [10]. Furthermore,

§ Present address: School of Physics and Astronomy, St Andrews University, North Haugh, St Andrews KY16 9SS, UK. Telephone: +44 1334 463159; fax: +44 1334 463104.

0953-8984/99/183687+11$19.50

high-resolution angle-resolved photoemission studies showed that the complicated magnetic structure of CeSb is strongly related to its unique electronic structure as predicted by the non-linear p–f mixing model [11].

In the present studies we have found that Ni atoms can be incorporated in the cubic unit cell of CeSb, and that thereby the physical properties are strongly affected. We present results of electron-probe microanalysis (EPMA), x-ray powder diffraction, magnetization, magnetic susceptibility and electrical resistivity measurements on $CeSbNi_{0.15}$ single crystal. Furthermore, we have also investigated the solubility limit of Ni in the polycrystalline alloys $CeSbNi_x$ ($x = 0$ to 0.5) using metallographic examination, EPMA and x-ray powder diffraction techniques, and have studied their magnetic and transport properties.

2. Experimental details

$CeSbNi_{0.15}$ single crystal was prepared by the Bridgman method using a molybdenum crucible sealed under a high-purity argon atmosphere by arc welding. The purities of the starting materials were 99.99% for Ce(Ni) and 99.999% for Sb. We started with the nominal composition '$CeSb_{1.6}Ni$'. An alloy of CeNi prepared by arc melting and an Sb ingot were directly loaded in the Mo crucible. In a vacuum furnace, the crucible was heated up to 1500 °C and pulled down with a velocity of 1.5 mm h^{-1}. Polycrystalline samples of $CeSbNi_x$ ($x = 0$ to 0.5) were prepared by arc melting stoichiometric amounts of the constituent elements (purity 99.99% for Ce, 99.95% for Ni and 99.999% for Sb) on a water-cooled copper hearth under a high-purity argon atmosphere. Using stoichiometric amounts, $CeNi_x$ alloys were arc melted and then these alloys were melted with an appropriate amount of Sb. Due to the volatile nature of Sb, about 5 wt% Sb was taken in excess during the first melting, which compensated for Sb losses. The compositions of the crystal and polycrystalline samples were determined by EPMA. X-ray powder diffraction studies were carried out using a MAC (Material Analysis and Characterization Science Company Limited, model MX-Labo) diffractometer with Cu Kα radiation at room temperature. The magnetic susceptibility was measured using a SQUID magnetometer (Quantum Design, CA) between 2 and 300 K in an applied field of 0.5 T. High-field magnetization measurements were carried out by an extraction method with dc fields up to 15 T at the Institute for Solid State Physics, University of Tokyo. Resistivity measurements were carried out using a standard four-probe dc technique between 1.3 K and 300 K. The typical dimensions of the resistivity samples were $1 \times 1.5 \times 4$ mm for the $CeSbNi_{0.15}$ single crystal and $1.5 \times 1.5 \times 6$ mm for the polycrystalline alloys. The current and voltage leads, made with Au wire of 50 μm diameter, were connected to the samples with electrically conductive silver paint. The constant dc current between 1 and 10 mA (obtained using a Keithley 220 programmable current source) was passed through the samples in both directions (positive and negative) to eliminate the thermal emf. The voltages were measured using a Keithley 182 sensitive digital voltmeter.

3. Results and discussion

Our crystal growth method gave many plate-like single crystals measuring approximately $1 \times 1.5 \times 4$ mm, at the bottom of the crucible. Laue x-ray diffraction patterns showed a cubic symmetry. EPMA of the single crystal showed the composition $CeSbNi_{0.15}$ without any impurity phase. We pulverized the crystal for x-ray powder diffraction studies, which revealed a cubic structure with the lattice parameter $a = 4.438(4)$ Å; the number in the parentheses shows the error. Figure 1 shows x-ray powder diffraction patterns of $CeSbNi_x$ polycrystalline alloys.

The XRD patterns of all of the alloys could be indexed with a cubic structure, except a few impurity peaks (less than 3%) for $x = 0$ to 0.4 alloys. For $x = 0.5$, we found several peaks of the second phase, which is the hexagonal CeNiSb phase [12]. This indicates that the solubility limit of Ni in CeSb is approximately $x = 0.4$. The compositions of the impurity phases detected from EPMA are Ce_3Sb_2 for $x = 0$, $CeNiSb_2$ for $x = 0.08$, $CeNi_2Sb_2$ for $x = 0.35$ and $CeNi_3$ for $x = 0.4$. The sizes of the impurity phases in $x = 0.15$ and $x = 0.25$ alloys were smaller than 3 μm; hence their compositions could not be determined. The estimated compositions of the main cubic phase are CeSb ($x = 0$), $CeSbNi_{0.07}$ ($x = 0.08$), $CeSb_{1.02}Ni_{0.13}$ ($x = 0.15$), $CeSbNi_{0.24}$ ($x = 0.25$), $CeSbNi_{0.32}$ ($x = 0.35$) and $CeSb_{0.99}Ni_{0.38}$ ($x = 0.4$). The analysis of the positions of the diffraction peaks ($10^\circ \leqslant 2\theta \leqslant 120^\circ$) using the CELL program from the software package of the MAC diffractometer gave the lattice parameters. The lattice parameter increases almost linearly with increasing Ni composition, x, at a rate $\mathrm{d}a/\mathrm{d}x = 0.0849$ Å (figure 2). A small increase in the unit-cell volume, $\Delta V/V = 0.65\%$, has been observed between $x = 0$ and 0.5.

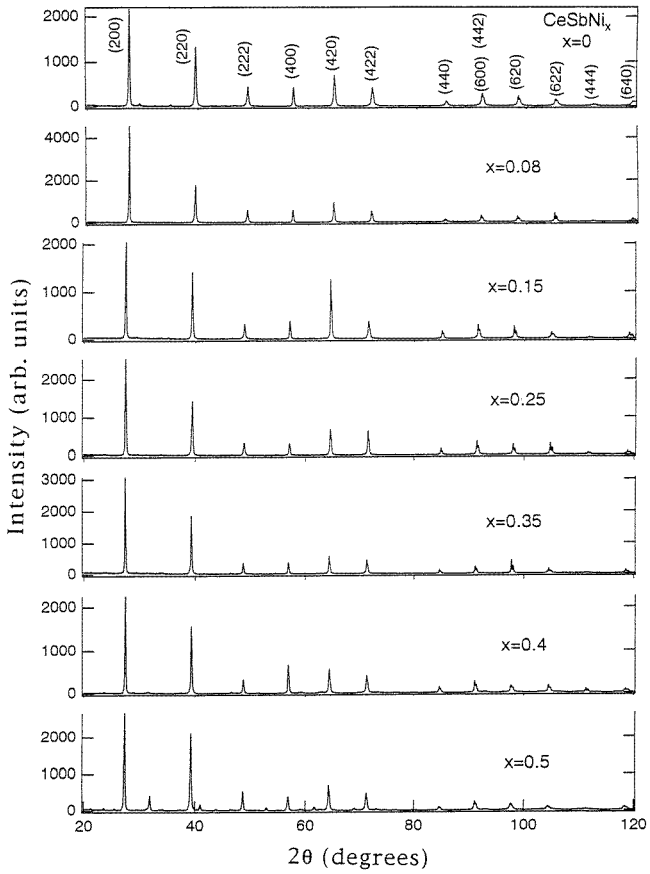

Figure 1. X-ray powder diffraction patterns of $CeSbNi_x$ ($0 \leqslant x \leqslant 0.5$) alloys obtained with Cu Kα radiation.

There is no obvious change in the diffraction pattern with x, as shown in figure 1. This fact suggests that the Ni atoms occupy the interstitial sites in the cubic NaCl-type structure. The anion sublattice of the NaCl structure has two empty tetrahedral holes per anion. Dwight [13]

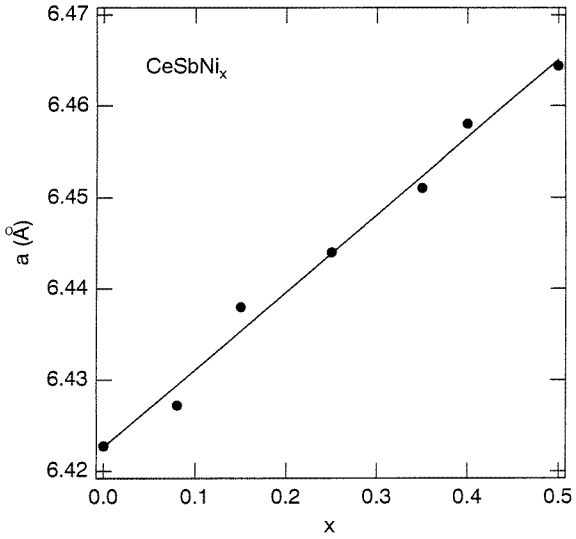

Figure 2. Lattice parameter a versus Ni concentration for $CeSbNi_x$ alloys. The solid line represents a linear behaviour.

has shown that it is possible to fill half of the holes surrounded by the Sb atoms with transition elements such as Ni and Pt, which gives the cubic MgAgAs-type structure (space group $F\bar{4}3m$, No 216). In fact, the compounds RNiSb with R = Gd to Lu have the cubic MgAgAs-type structure, while those with R = La to Sm have the hexagonal ZrBeSi-type structure [12, 13]. Therefore, there exist two possibilities for the structure of $CeSbNi_x$ alloys:

(a) if interstitial Ni atoms partially occupy the tetrahedral holes without distorting the cube cell, then the cubic MgAgAs-type structure may form;
(b) if interstitial Ni atoms distort the cubic cell by pushing out either Ce or Sb atoms, then a super-cell may form.

To check the former possibility, we simulated the x-ray powder diffraction pattern of $CeSbNi_x$ for $x = 0, 0.15, 0.4$ and 1.0 on the basis of MgAgAs-type structure using the RIETAN program [14]. Our simulation revealed that with increasing Ni occupancy of the 4c site, the intensity of the strongest (200) peak decreases, while that of the (220) peak increases. Between 35% and 40% Ni occupancy, the intensities of the (200) and (220) peaks are almost equal, while for 100% Ni occupancy, the (220) peak has the highest intensity and the (200) peak has an intensity that is about 60% of that of the strongest peak. However, our x-ray diffraction patterns (figure 1) do not follow this type of intensity variation, which ruled out the possibility of MgAgAs-type structure with partially occupied Ni atoms at the 4c sites. Hence, we believe that a super-cell forms in $CeSbNi_x$, even though the superlattice reflections were not clearly observed. We recall here that a super-cell forms in cubic $CePd_3$ when Ga, In, Sb, Bi and Pb atoms are incorporated [15]. To check for the presence of the super-cell in the present system, detailed neutron scattering measurements on a single-crystal sample are essential.

Figure 3 shows the magnetic susceptibility versus temperature for $CeSbNi_{0.15}$ single crystal for $\boldsymbol{B} \parallel [100]$ and $\boldsymbol{B} \parallel [110]$ and the inset shows the low-temperature behaviour. A peak in the susceptibility at 9.5 K for both $\boldsymbol{B} \parallel [100]$ and $\boldsymbol{B} \parallel [110]$ indicates an antiferromagnetic ordering of the Ce moments. The Néel temperature, $T_N = 9.5$ K, is lower than $T_N = 16$–18 K (first-order transition) for the host CeSb [5]. The zero-field-cooled (ZFC) and field-cooled

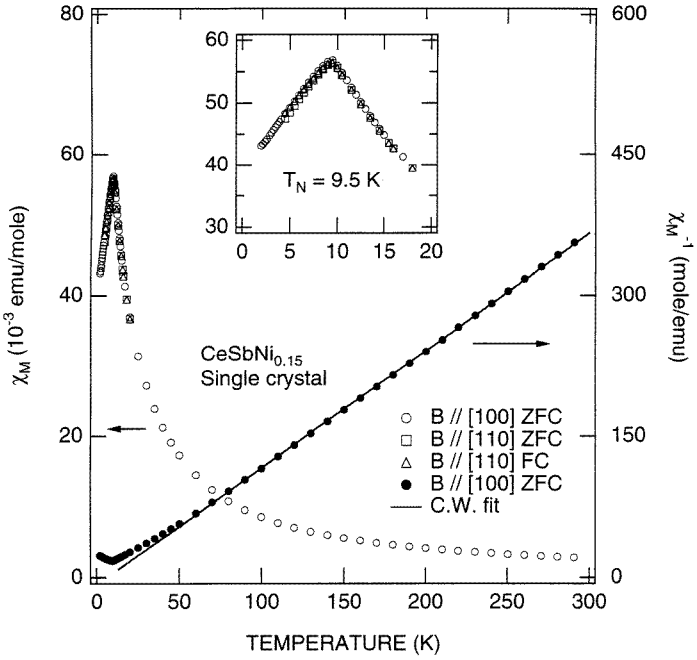

Figure 3. Magnetic susceptibility versus temperature for $CeSbNi_{0.15}$ single crystal in an applied field of 0.5 T for $\boldsymbol{B} \parallel [100]$ and $\boldsymbol{B} \parallel [110]$. The secondary y-axis shows the inverse susceptibility and the solid line represents Curie–Weiss behaviour. The inset shows the low-temperature behaviour.

(FC) susceptibilities are identical, which further confirms antiferromagnetic ordering rather than a spin-glass transition: for a spin-glass system, ZFC susceptibility exhibits a peak, which disappears in FC susceptibility [16]. The susceptibility exhibits Curie–Weiss (C–W) behaviour between 300 and 60 K with an effective magnetic moment $\mu_{eff} = 2.54(0.02)\ \mu_B$ and a paramagnetic Curie temperature $\theta_p = 6.1(0.3)$ K. These values are comparable with $\mu_{eff} = 2.56$–$2.58\ \mu_B$ and $\theta_p = 5$–8 K for CeSb [5]. The observed value of μ_{eff} is the same as is expected for the free Ce^{3+} ion with $J = 5/2$, which indicates that the nickel atoms do not carry magnetic moments. The observed positive sign of θ_p for $CeSbNi_{0.15}$ and CeSb suggests ferromagnetic-type correlations between the Ce moments at high temperatures, which is unusual for an antiferromagnetic ground state. The observed deviation from C–W behaviour below 70 K (figure 3) is attributed to the crystalline-electric-field effect on the ground-state multiplet $J = 5/2$ of the Ce^{3+} ion which splits into a doublet and a quartet under the cubic crystal field. We have also measured the magnetic susceptibility of the polycrystalline $CeSbNi_x$ ($x = 0$ to 0.4) alloys between 2 and 20 K (figure 4(a)) in order to investigate the variation of T_N with the Ni concentration, x. The temperature dependence of the susceptibility of CeSb exhibits two peaks at 16 K and 4.6 K, which agree well with previous studies [5]. The susceptibility of the $x = 0.08$ alloy also exhibits two peaks at 9.5 K and 3.6 K. Furthermore, the susceptibilities of the $x = 0.15$, 0.25, 0.35 and 0.4 alloys each show only one peak, at 9.5, 10.5, 10.5 and 12.5 K, respectively. T_N was estimated from the position of the peak, which exhibits non-linear variation with the Ni concentration (figure 4(b)). T_N decreases sharply from 16 K for $x = 0$ to 9.5 K for $x = 0.08$ and then remains almost constant up to $x = 0.15$ ($T_N = 9.5$ K). On further increase in the Ni concentration, T_N increases with x:

$T_N = 12.5$ K for $x = 0.4$. We also measured the high-temperature susceptibilities of $x = 0.35$ and $x = 0.4$ alloys. The susceptibility, for both alloys, exhibits C–W behaviour down to T_N, with $\mu_{eff} = 2.57(0.02)\ \mu_B$ and $\theta_p = -3.5(0.2)$ K for $x = 0.35$, and $\mu_{eff} = 2.58(0.02)\ \mu_B$ and $\theta_p = -2.2(0.1)$ K for $x = 0.4$.

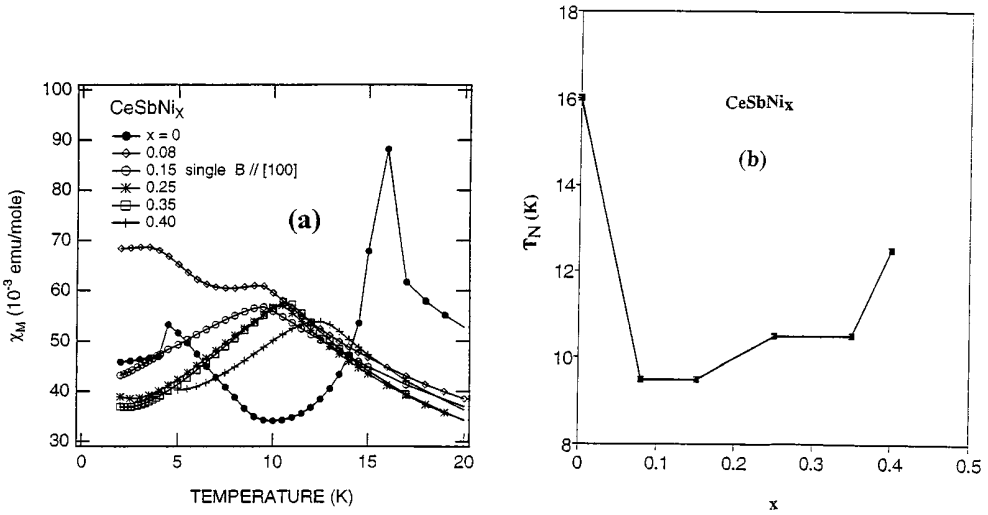

Figure 4. (a) Magnetic susceptibility versus temperature for CeSbNi$_x$ ($x = 0$ to 0.4) polycrystalline alloys and CeSbNi$_{0.15}$ single crystal for $\boldsymbol{B} \parallel [100]$ in an applied field of 0.5 T. (b) The Néel temperature, T_N, versus the Ni composition, x.

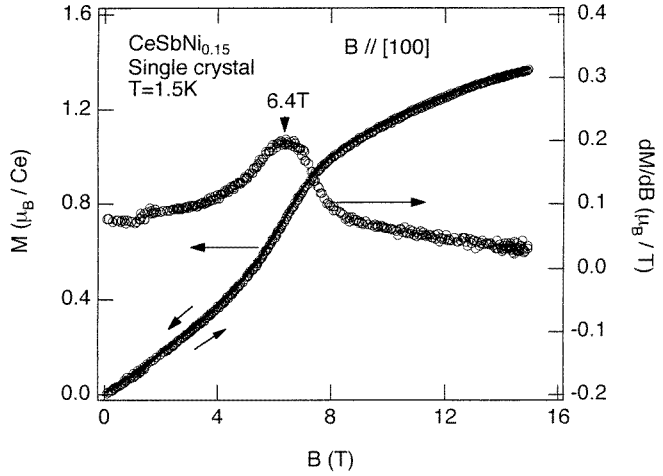

Figure 5. Magnetization versus applied field for CeSbNi$_{0.15}$ single crystal for $\boldsymbol{B} \parallel [100]$ at 1.5 K. The secondary y-axis shows the differential magnetization $\mathrm{d}M/\mathrm{d}B$ versus B.

Figure 5 shows the magnetization isotherm of CeSbNi$_{0.15}$ along the [100] axis at 1.5 K. The magnetization increases linearly up to 4 T, and deviates upward and eventually shows partial saturation at higher fields. No complete saturation, as seen in CeSb (see the inset in figure 6), was observed up to 15 T. The value of the magnetic moment at 15 T is 1.36 μ_B,

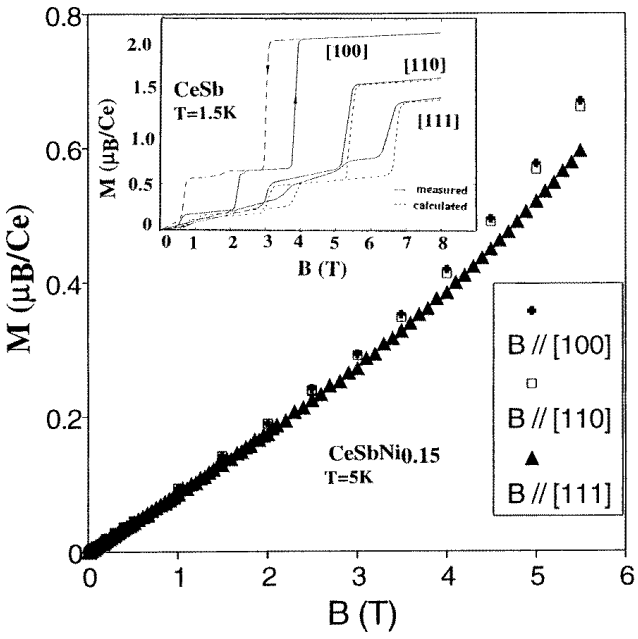

Figure 6. Magnetization versus applied field for $CeSbNi_{0.15}$ single crystal for $\boldsymbol{B} \parallel [100]$, $\boldsymbol{B} \parallel [110]$ and $\boldsymbol{B} \parallel [111]$ at 5 K. The inset shows the magnetization versus the applied field at 1.5 K for CeSb single crystal [20].

which is less than the value 2.05 μ_B/f.u. observed for CeSb for $\boldsymbol{B} \parallel [100]$ [5]. The plot of $\mathrm{d}M/\mathrm{d}B$ exhibits a broad peak at 6.4 T due to the metamagnetic transition, which is probably of the spin-flip type. It is worthwhile mentioning here that the magnetization of CeSb for $\boldsymbol{B} \parallel [100]$ at 1.5 K exhibits three metamagnetic transitions at 0.5, 2 and 3.7 T, respectively, with large hysteresis [5]. Furthermore, the magnetization of CeSb at 1.5 K exhibits strong anisotropy for the $\boldsymbol{B} \parallel [100]$, $\boldsymbol{B} \parallel [110]$ and $\boldsymbol{B} \parallel [111]$ directions; see the inset in figure 6. To check for possible anisotropy in the magnetization of $CeSbNi_{0.15}$ single crystal, we measured the magnetization for the $\boldsymbol{B} \parallel [100]$, $\boldsymbol{B} \parallel [110]$ and $\boldsymbol{B} \parallel [111]$ directions at 5 K up to a field of 5.5 T using a SQUID magnetometer (figure 6). The magnetization increases linearly with field in all three directions up to 4 T and deviates upward at higher fields. The magnetization for $\boldsymbol{B} \parallel [100]$ and $\boldsymbol{B} \parallel [110]$ exhibits similar behaviour, while weak anisotropy was observed at high fields for $\boldsymbol{B} \parallel [111]$.

Figure 7 shows the resistivity, ρ, versus temperature for $CeSbNi_{0.15}$ single crystal for $\boldsymbol{I} \parallel [100]$ and the inset shows the low-temperature behaviour. $\rho(T)$ decreases linearly with decreasing temperature down to 150 K and exhibits a curvature below this and eventually increases sharply below 10 K (see the inset of figure 7). At around 2 K, $\rho(T)$ exhibits a weak maximum. The sharp rise in $\rho(T)$ below 10 K is attributed to the formation of an antiferromagnetic superzone gap in the conduction band [17]. In contradiction to this behaviour, the resistivity of CeSb starts to decrease at a temperature well above T_N with a further drop at T_N.

The resistivity behaviour of the $CeSbNi_{0.15}$ polycrystalline sample is very similar to that of the single crystal, except that the low-temperature rise is less pronounced (figure 8). The absolute value of ρ at 300 K for the $x = 0.15$ alloy is 289 $\mu\Omega$ cm, which agrees well with that observed for the single-crystal sample. The observed high values of ρ at 300 K for the $x = 0.08$

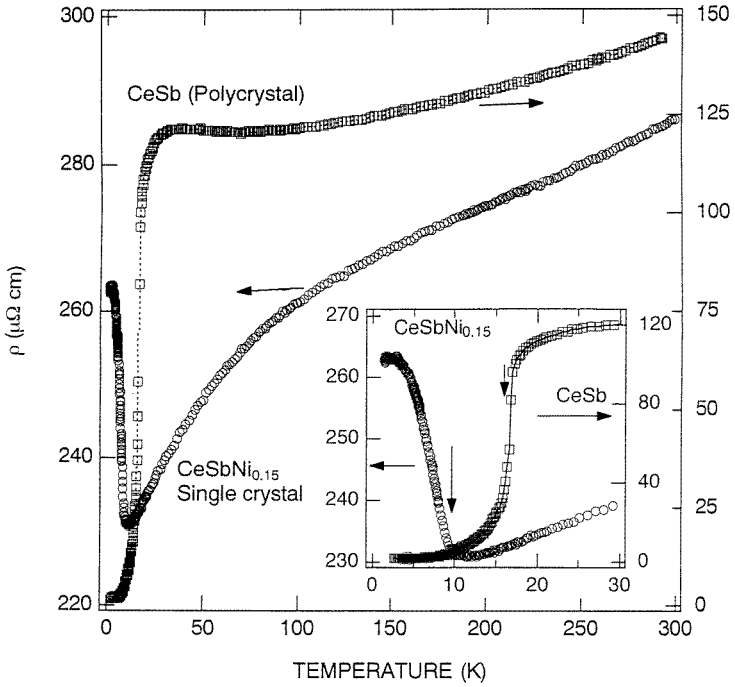

Figure 7. Resistivity versus temperature for $CeSbNi_{0.15}$ single crystal for $\boldsymbol{I} \parallel [100]$ and CeSb polycrystal. The inset shows the low-temperature behaviour. Vertical arrows represent the Néel temperature determined from magnetic susceptibility measurements.

(718 $\mu\Omega$ cm), 0.25 (554 $\mu\Omega$ cm), 0.35 (457$\mu\Omega$ cm) and 0.4 (557 $\mu\Omega$ cm) alloys are attributed to the presence of micro-cracks. Thus, the resistivity data for the polycrystalline alloys (in figure 8) are normalized to the room temperature value: $\rho(T)/\rho(300)$. The normalized $\rho(T)$ for all of the alloys exhibits a minimum followed by a broad maximum at low temperatures. A careful look at the composition dependence reveals some interesting features. The temperatures at which the minimum and maximum occur are the lowest for $x = 0.15$, and increase either side, which suggests non-linear variation of T_N with the Ni concentration, x. This has been confirmed through our susceptibility measurements on alloys with $x = 0$ to 0.4: T_N obtained from the susceptibility measurements is marked by a vertical arrow in figure 8. The low-temperature resistivity behaviour of the $x = 0.08$ alloy is very similar to that observed for $Ce_{0.85}La_{0.15}Sb$ [2]. It is to be noted that the resistivity starts rising slightly above T_N for $x = 0.25$, $x = 0.35$ and $x = 0.4$, which is expected for antiferromagnetic systems [18]. Furthermore, the low-temperature rise in ρ is maximum for the $x = 0.25$ alloy. These results demonstrate the significant change of the band structure and the Fermi surface topology with x.

4. Conclusions

We have prepared single crystals of the new ternary compound $CeSbNi_{0.15}$. This compound crystallizes in the cubic structure, like the host compound CeSb, with Ni atoms occupying the interstitial sites. The magnetic susceptibility measurements on the single crystal for $\boldsymbol{B} \parallel [100]$ and $\boldsymbol{B} \parallel [110]$ reveal an antiferromagnetic ordering at $T_N = 9.5$ K. The magnetization isotherm at 1.5 K shows a metamagnetic transition at a field of 6.4 T. The magnetizations at 5 K for the

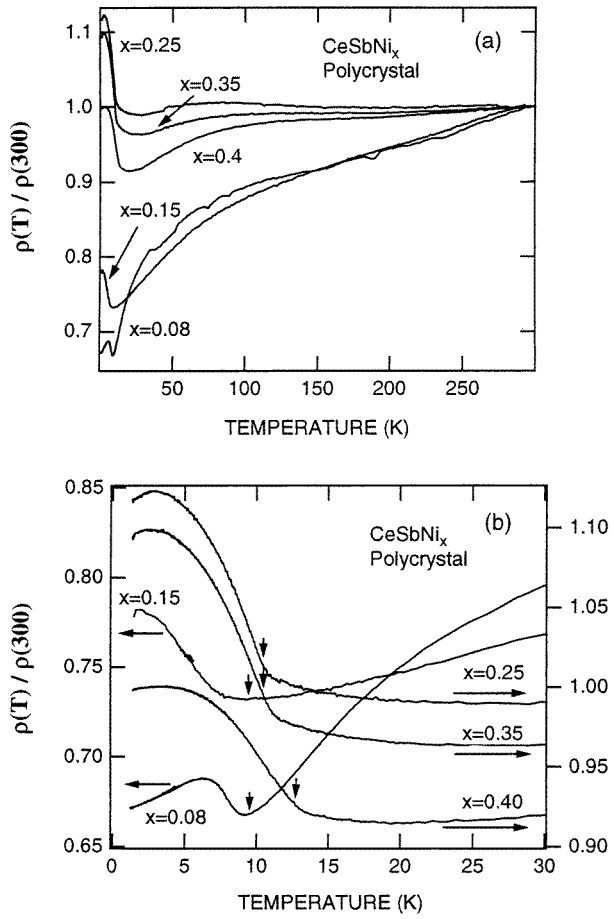

Figure 8. Normalized resistivity versus temperature for $CeSbNi_x$ polycrystalline alloys. The data are normalized to the value of ρ at 300 K (see the text). The vertical arrows represent the Néel temperatures determined from magnetic susceptibility measurements.

$\boldsymbol{B} \parallel [100]$, $\boldsymbol{B} \parallel [110]$ and $\boldsymbol{B} \parallel [111]$ directions show almost similar behaviour up to 5.5 T. The resistivity exhibits a sharp rise below T_N, indicating the formation of a superzone gap. It is well established that the Fermi energy in CeSb is comparable to the energy of mixing between 4f and conduction electrons [3]; hence the Sb 5p(holes)–Ce 4f(Γ_8) mixing effect is strongly non-linear, which is the origin of the anomalous and complex magnetic properties of this material. For $CeSbNi_{0.15}$, however, the absence of strong anisotropy along with a simple field dependence of the magnetization suggests that the p–f mixing has collapsed with Ni incorporation. A very similar change in the magnetic properties has been observed for $CeSb_{1-x}Te_x$ alloys [19]. The collapse of the p–f mixing in $CeSbNi_x$ could arise through an overlap between the p band of Sb and the d band of Ni, which fills the p holes that mix strongly with the Γ_8 state of Ce. Furthermore, it is to be noted that the change in the physical properties of $CeSbNi_x$ alloys is also expected due to the volume expansion with x, which produces a negative chemical pressure, and disorder introduced by Ni atoms. To check on these points, high-resolution angle-resolved photoemission studies as well as inelastic neutron scattering measurements are essential.

To determine the solubility limit of Ni in CeSb, we have also synthesized polycrystalline alloys, $CeSbNi_x$ ($x = 0.08$, 0.15, 0.25, 0.35, 0.4 and 0.5). Our EPMA and x-ray diffraction studies showed that the solubility limit of Ni is about 40%. The cubic lattice parameter increases almost linearly with the Ni concentration, with a volume expansion of 0.65% for $x = 0.5$. The magnetic susceptibility reveals the non-linear variation of T_N with x. The resistivity of each of these alloys shows a sharp rise at low temperatures, which we attribute to superzone-gap formation.

Acknowledgments

One of us (DTA) is grateful to the Japan Society for the Promotion of Science (JSPS) for the award of a research fellowship. We acknowledge T Suzuki for useful discussions. We thank F Iga and I Oguro for the magnetization measurements performed at the Materials Design and Characterization Laboratory, Institute for Solid State Physics, University of Tokyo. We wish to thank T Fujita and T Suzuki for allowing us generous use of their SQUID susceptometer.

References

[1] Kasuya T, Takegahara K, Aoki Y, Suzuki T, Kunii S, Sera M, Sato N, Fujita T, Goto T, Tamaki A and Komatsubara T 1982 *Valence Instabilities* ed P Wachter and H Boppart (Amsterdam: North-Holland) p 359
[2] Sera M 1982 *PhD Thesis* Tohoku University
[3] Suzuki T 1993 *Japan. J. Appl. Phys.* **8** 267
[4] Kasuya T, Sera M, Okayama Y and Hagay Y 1996 *J. Phys. Soc. Japan* **65** 160
[5] Rossat-Mignod J, Burlet P, Villain J, Bartholin H, Wang Tcheng-Si and Florence D 1977 *Phys. Rev.* B **16** 440
Rossat-Mignod, Burlet P, Quezel S, Effantin J M, Delacôte D, Bartholin H, Vogt O and Ravot D 1983 *J. Magn. Magn. Mater.* **31–34** 398
Busch G and Vogt O 1967 *Phys. Lett.* A **25** 449
Tsuchida T and Nakamura Y 1968 *J. Phys. Soc. Japan* **25** 284
[6] Chattopadhyay T, Burlet P, Rossat-Mignod J, Bartholin H, Vettier C and Vogt O 1986 *J. Magn. Magn. Mater.* **54** 503
Chattopadhyay T, Burlet P, Rossat-Mignod J, Bartholin H, Vettier C and Vogt O 1987 *J. Magn. Magn. Mater.* **63+64** 52
[7] Hor P H, Meng R L, Yomo S, Chu C W, Bucher E and Schmidt P H 1986 *Physica* B + C **139** 378
[8] Hulliger F, Landolt M, Ott H R and Schmelczer R 1975 *J. Low Temp. Phys.* **20** 269
[9] Rainford B, Turberfield K C, Busch G and Vogt O 1968 *J. Phys. C: Solid State Phys.* **1** 679
Busch G, Stutius W and Vogt O 1971 *J. Appl. Phys.* **42** 1493
Heer H 1975 *Eidgenössische* Institut für Reaktotechnik, AF. SSP. 84, Würenlingen (unpublished)
[10] Kasuya T 1985 *Theory of Heavy Fermion and Valence Fluctuations* ed T Kasuya and T Saso (Berlin: Springer) p 2
Takahashi H, Takegahara K, Yanase A and Kasuya T 1982 *Valence Instabilities* ed P Wachter and H Boppart (Amsterdam: North-Holland) p 359
Kasuya T 1995 *Physica* B **215** 88
[11] Takahashi T, Kumigashira H, Kim H D, Ashihara A, Chainani A, Yokoya T, Uesawa A and Suzuki T 1998 *J. Magn. Magn. Mater.* **177–181** 1027
[12] Hartjes K and Jeitschko W 1995 *J. Alloys Compounds* **226** 81
[13] Dwight A E 1974 *Proc. 11th Rare Earth Conf. (Traverse City, MI)* p 642
[14] Izumi F 1993 *The Rietveld Method* ed R A Young (Oxford: Oxford University Press)
[15] Gordon R A and DiSalvo F J 1996 *Z. Naturf.* b **51** 52
Gordon R A, Jones C D W, Alexander M G and DiSalvo F J 1996 *Physica* B **225** 23
[16] Mydosh A J 1993 *Spin Glasses: an Experimental Introduction* (London: Taylor and Francis)
[17] Elliott R J and Wedgewood F A 1963 *Proc. Phys. Soc.* **81** 846
[18] Ueda K 1977 *J. Phys. Soc. Japan* **43** 1497
[19] Ravot D, Percheron-Guegan A, Durand J M, Olivier-Fourcade J, Jumas J C and Parent P 1997 *J. Alloys Compounds* **261** 12
[20] Busch G and Vogt O 1967 *Phys. Lett.* A **25** 449